Application of CFD to Explain Anomalous Stall Behavior of the SSME Flowmeter

E Ascoli, W. Clever, A. Hadid, E. D. Lynch, M. Stewart, and
CFD Technology Center
Rocketdyne Propulsion and Power
The Boeing Company
and K. Lee
Rockwell International Science Center

IN-34
046442

1. Background of SSME Flowmeter Behavior

The Space Shuttle Main Engine (SSME) Fuel Flowmeter is located in the duct between the low and high pressure fuel turbopumps. In the flowmeter the rotation rate of a 4-blade rotor positioned downstream of two flow straighteners is employed to measure the engine fuel flow rate and thereby control the engine mixture ratio via the engine controller. Hence, inaccurate operation of the flowmeter could have serious consequences for SSME engine operation and performance, forcing, for example, tanking of extra fuel to allow for inaccurate flowmeter measurement.

Since the current flight flowmeter configuration was incorporated into the SSME in the early eighties, some anomalies in flowmeter behavior have been observed. The initial flowmeter incorporated an "egg crate" design for the two flow straighteners which turn the duct flow to make it more uniform and parallel after it has come out of the 90° bend just upstream of the

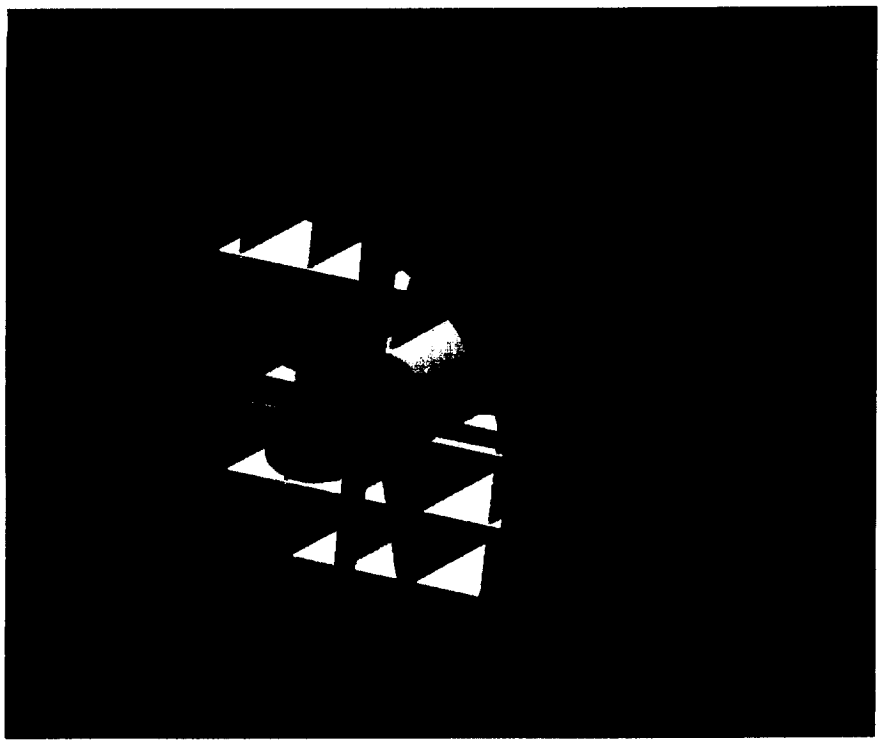

Figure 1: Egg Crate Flowmeter Configuration

flowmeter. In the egg crate, the vanes of the flow straightener were in a rectangular configuration (see Figure 1) and at no point did the wake of the vanes line up with the rotor blade.
The vanes in the current flow straighteners are in a hexagonal web configuration (see Figure 2) allowing the wakes to line up with rotor blade; moreover, for reasons of structural support, the rotor–straightener distance has been reduced in the present design by approximately half when

compared with the egg crate design, thereby increasing the extent of fluid dynamic wake interactions.

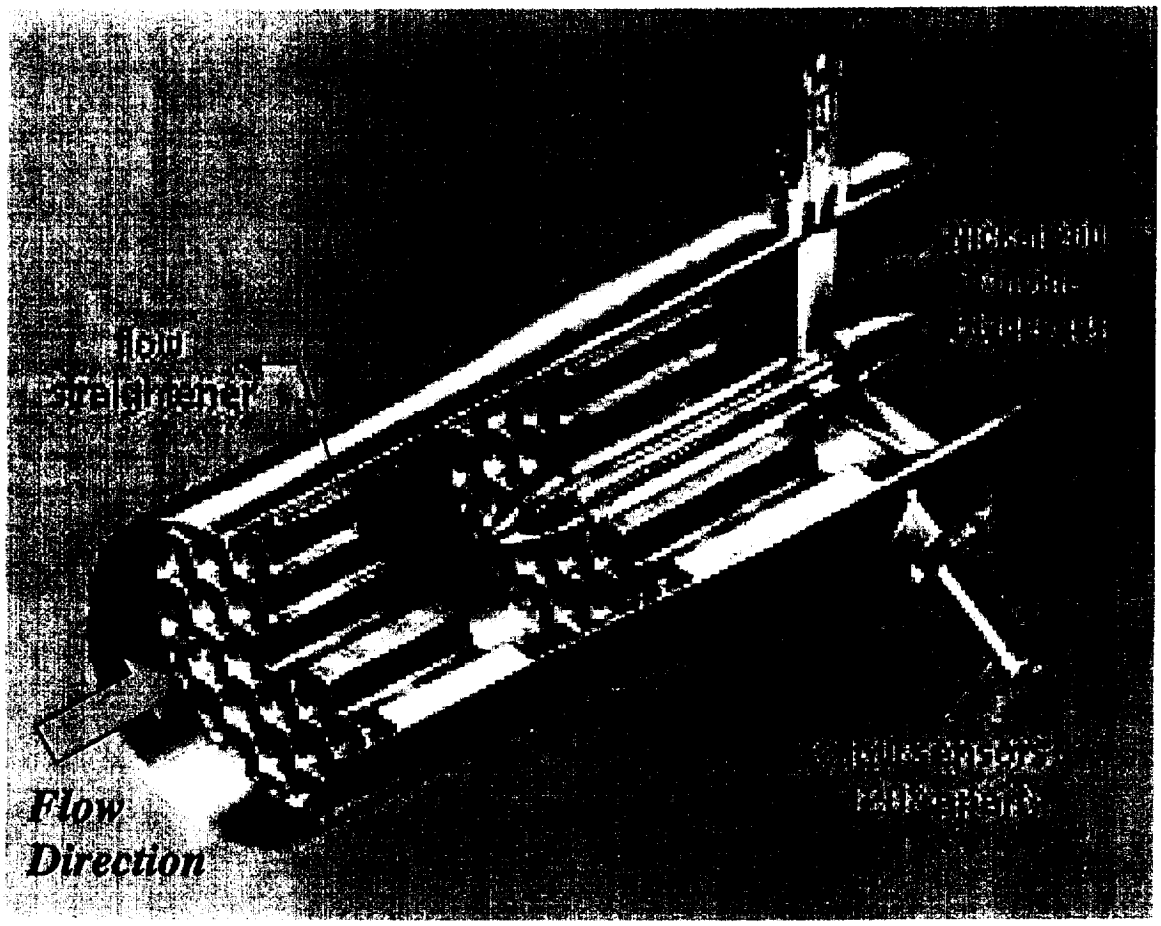

Figure 2: Current Flowmeter Configuration

Two types of "anomalies" have been observed with the present design, flowmeter constant K_f "shifting" and flowmeter "aliasing". The aliasing phenomena is illustrated in Figure 3 in which the perceived engine flowrate begins to oscillate with a large amplitude and perceived low frequency. This is always accompanied by the phenomena shown in Figure 4 where the previously calibrated flowmeter constant seems to "shift," upon which the engine controller changes the mixture ratio to accommodate what it thinks is a change in fuel flowrate, but is actually an artifact of a change in the behavior of the flowmeter.

One explanation for this type of behavior is that the fluid dynamic forces on the blade have become unsteady at a relatively low frequency, causing the blade to bend with these unsteady forces or to rotate at an oscillatory speed as the lift and drag on the blade vary periodically and affect the blade rotation through the balance of torques on the blade. The possibility of the blade bending periodically and affecting the sensor measurements in a manner required to cause the observed test results has been largely ruled out through observing that all four blades of the rotor act in phase, suggesting that the rotor rotates as a rigid body, but at a sinusoidal speed.

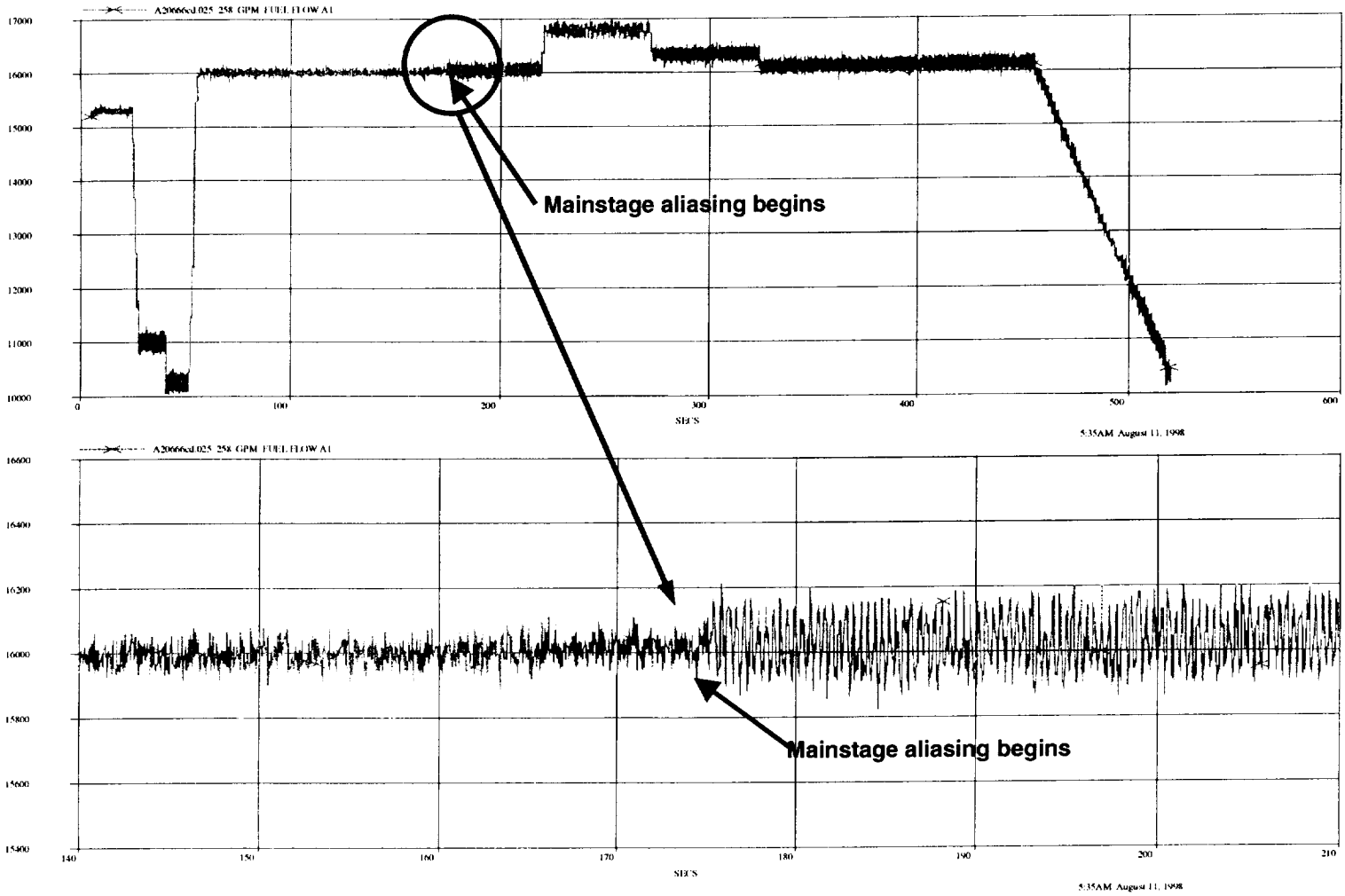

Figure 3: Flowmeter Aliasing

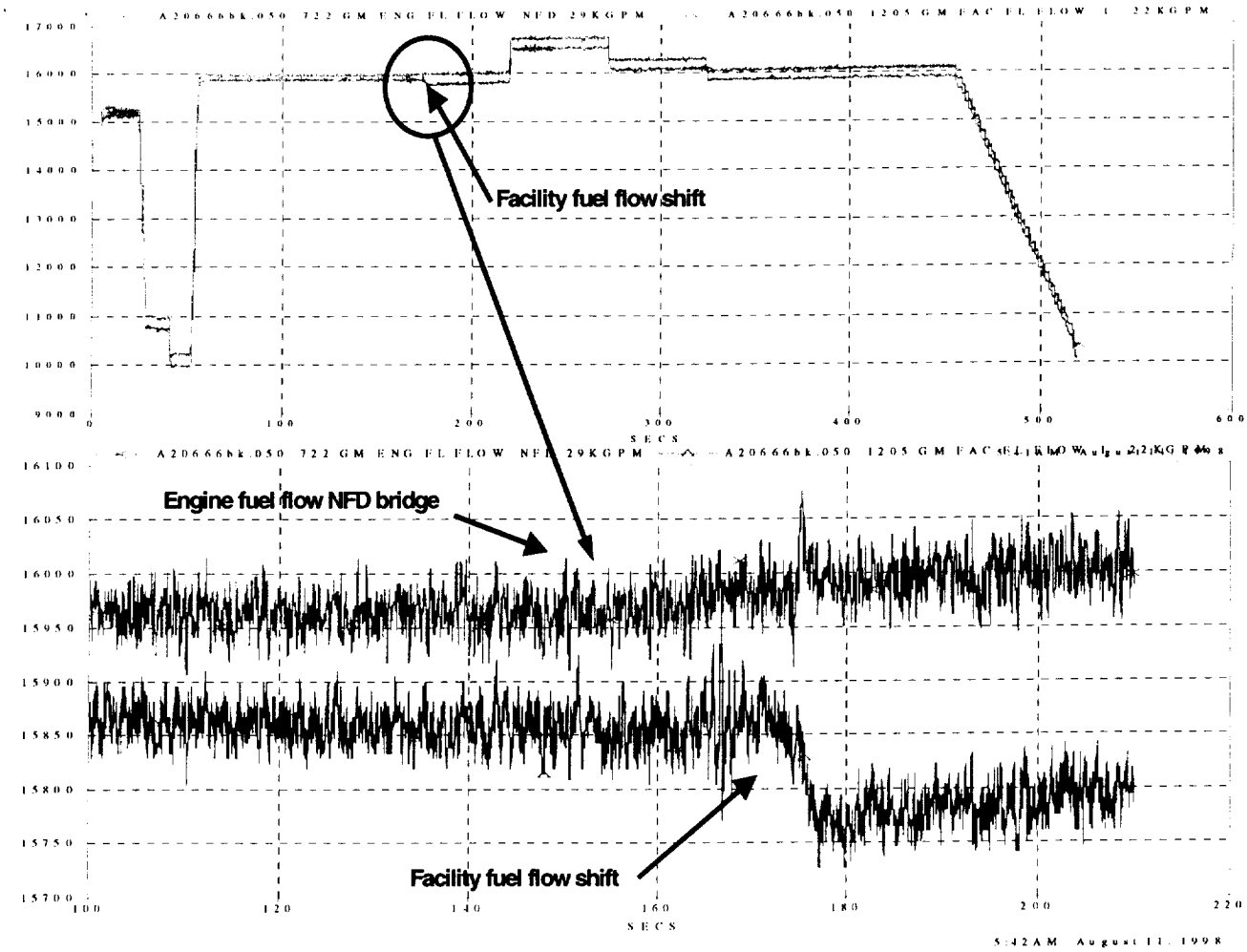

Figure 4: Flowmeter Shifting

2. Description of and Approach to Analysis of Flowmeter Flow Physics

Based on this information, an engineering team was set up to "brainstorm" the possibilities for the cause of flowmeter shifting and aliasing. A key hint at the cause was the observed constant conjunction between these two types of behavior. A range of similar scenarios were proposed for how wake interactions might initiate shifting.

One such hypothesis is that because of the greater velocity deficit for the current straightener vane wakes, the angle-of-attack (AOA) on the blade rises, the Reynolds number on the blade decreases, and the blade stalls. From existing correlations for airfoils, the Strouhal number for two-and three-dimensional stall instabilities should be respectively approximately .02 and .045, yielding frequencies of respectively 170 Hz and 390 Hz after accounting for the reduced velocity in the wakes; on the other hand, the Strouhal number for Karman bluff body shedding is approximately .15, making the shedding frequency in the absence of wakes 2200 Hz. The stall hypothesis was observed to be consistent with test observations: the observed frequency was at a relatively low frequency like those in test (but will not be reproduced precisely because of the low test sampling rate) and would decrease as wake interactions were diminished as was observed in the egg crate.

Hence, an approach was put forth to increase the confidence level in this hypothesis. First a two-dimensional CFD model of the flowmeter would be analyzed to ascertain whether the design modification could have indeed caused the assumed stall behavior. At this point, a design concept compatible with the current flowmeter concept yet modified to eliminate stalling would be formulated, and a three-dimensional CFD model would be analyzed to serve as a "proof-of-concept" for the design.

An alternative approach to a "proof-of-concept" test/analysis would be a cold flow test. However, a quick look at the required test conditions indicate this is an extremely challenging alternative because of the small rotor thickness and length (.1 in and .75 in respectively), rotational reference frame, enormous liquid velocity (of order 250 ft/s) and consequent large Reynolds number (of order 10^7). Hence, when facility options for cold flow testing appeared limited, the decision was made to proceed to a full engine test after completing a detailed CFD analysis.

3.Two-Dimensional CFD Model of Flowmeter Operation

The two-dimensional, unsteady CFD model of the flowmeter operation (geometry and computational grid) is shown in Figure 5. The rotor was kept stationary and the straightener

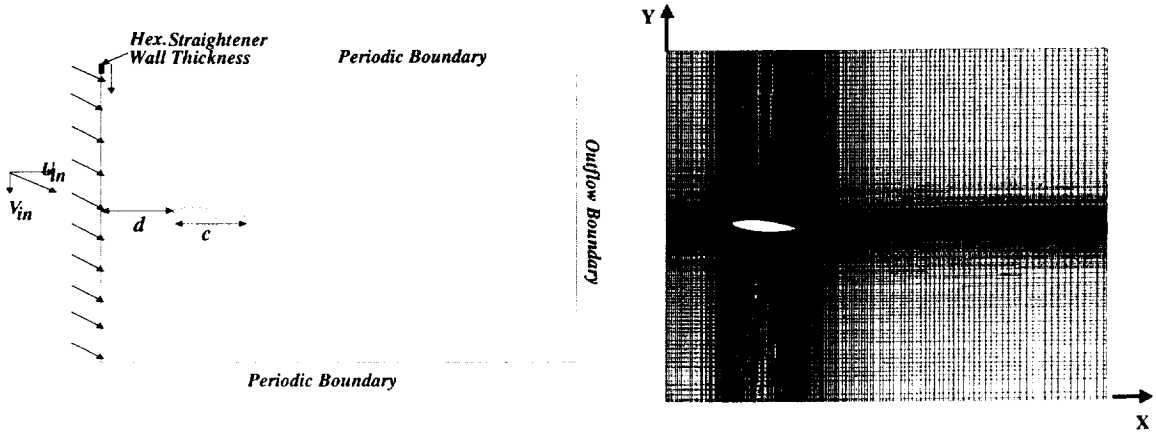

Figure 5: Two-Dimensional Computational Geometry and Grid

(idealized in two dimensions as a backward step) was treated as an obstacle and moved relative to the rotor. The PISO time-accurate pressure correction methodology was employed and the time step was tested to ensure time accuracy. Incompressible flow was assumed at the 64% power level.

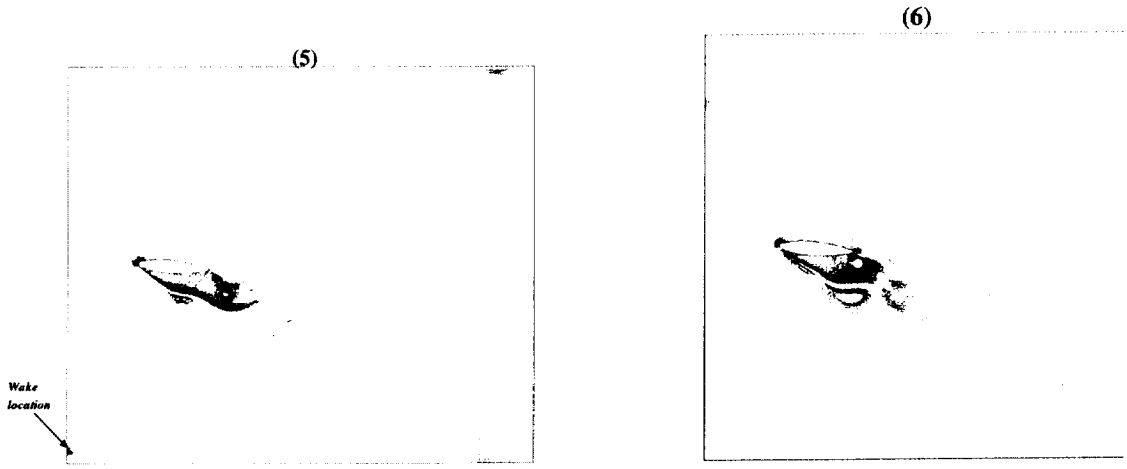

Figure 6: Velocity Magnitude Past Rotor Showing Separated Stall

Two slices in time of this series of computations is shown in Figure 6. A separation of the boundary layer is set up on the suction side of the blade, indicating that the blade flow is not described by a simple potential flow plus boundary layer approximation; this separation periodically detaches from the blade, creating a periodic disturbance. As indicated in Figure 7 presenting the power spectral density of this flow, the frequency of this disturbance (i.e., 130 Hz) matches almost exactly that expected for two-dimensional stall disturbances. Moreover, this disturbance is seen to disappear as the rotor–straightener spacing is increased to that employed in the egg crate design. As the stalling disturbance is eliminated, vortex shedding at approximately 2200 Hz comes more into play. Also apparent is the wake passing frequency of approximately 800 Hz and its harmonics.

The results of the two-dimensional CFD analysis suggested cutting back the flow straightener to the previous egg crate distance, eliminating the wake induced stall phenomena. However, this approach would leave the rotor with too little structural support. Therefore, a concept was proposed which would cutback the straightener at an angle, leaving the straightener similar to the existing configuration along the hub where the rotational velocity and angle-of-attack are necessarily small and increasing the distance between the rotor and the straightener until it matched the egg crate distance at the tip. Two three-dimensional CFD analyses were then conducted to observe the improvement relative to the existing design.

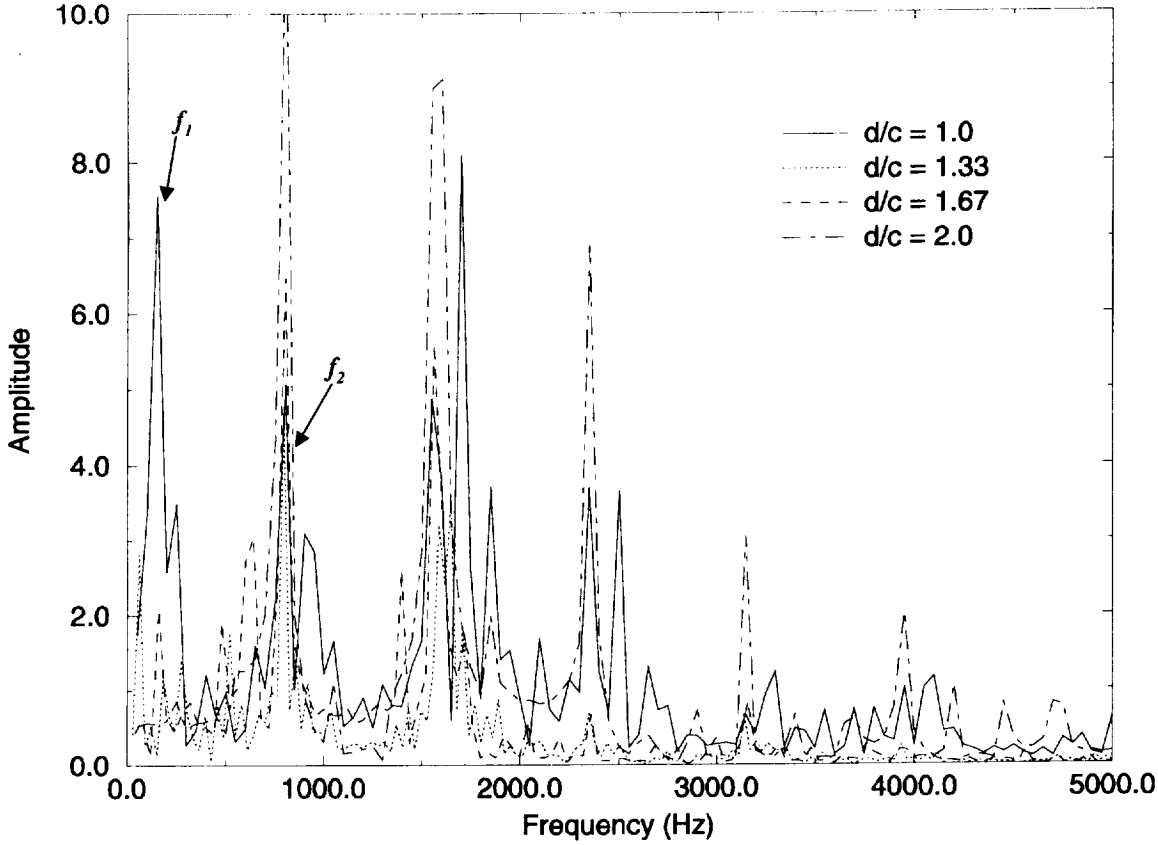

Figure 7: Power Spectral Density Showing Stall Disappearing as Rotor–Straightener Distance is Increased

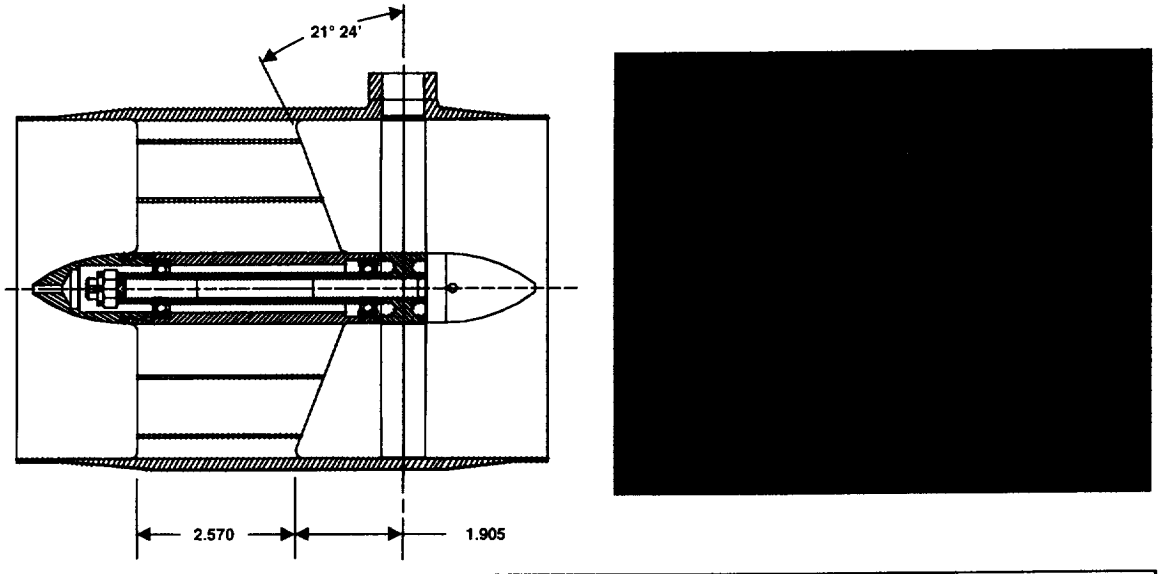

Figure 8: Proposed Cutback Flowmeter Configuration

4. Three-Dimensional CFD Model of Flowmeter Operation

Three-dimensional CFD models of both the cutback and existing flowmeter configurations were constructed to confirm the stalling characteristics of the proposed design. The 92-zone computational model of a 120-degree sector of the existing flowmeter is illustrated in Figure 8. To take advantage of its unaligned grid and time-accurate capabilities, the CFD solutions were run with the USA code as perfect gases at low Mach number to approximate the compressible liquid (i.e., LH_2 in the flowmeter). The rotation of the rotor was treated through the boundary conditions on the rotor. Because a truly unsteady approach involving moving the rotor would have not met program schedule and cost requirements, the rotor was treated as "pseudounsteady"; i.e., the blade was fixed at three representative positions and the consequent unsteady flow was then observed.

Figure 9 shows particle traces of the flow coming out of the straightener and past the rotor. The flowfield set up about the rotor when the blade is positioned in the wake is extremely similar to that observed in the previous two-dimensional "truly unsteady" analysis (Figure 11). As is seen in Figures 12 and 13 showing the wake velocity for both the existing and cutback flowmeters, the rotor sets up a pressure gradient for the pressure relative to the suction side of the blade which affects the upstream flow.

The diminished wake intensity for the cutback configuration (Figure 13) results in reduced stalling characteristics for the flow for the first two blade positions tested. For position 1 where the rotor was lined up directly with the flow straightener vane wakes the stalling oscillations in the blade lift coefficient (which controls the blade rotation speed) (cf. Figure 14), are considerably diminished in the cutback configuration as illustrated by the power spectral density of the lift coefficient (Figures 15, 16).

At position 2 where the blade crosses the vane wake, the situation is even more interesting. When the drag coefficient is plotted against the lift coefficient to describe the "state" of the flow about the rotor, the flow in the existing configuration is observed to approach a singly periodic state with a frequency much lower than that expected for vortex shedding. However, at some point this approach to a limit cycle is disturbed and the rotor flow jumps to another state—much as this same behavior is observed in flowmeter tests. By contrast the cutback shows no evidence of stall-like behavior for position 2.

5. Summary

High fidelity CFD analysis has led to an understanding of the flowmeter "aliasing" and "shifting" as being the result of periodic stalling of the rotor blades. The predicted behavior agrees with all characteristics observed in testing including the seeming randomness of the transition to the "shifted" flowmeter state. A design "fix" has been developed which takes account of what was learned from CFD; plans are to hot-fire test this "fix" in 1999. Thus a critical engine issue has been resolved largely through the application of advanced analysis tools, in particular, computational fluid dynamics.

Computational Grid for Three-Dimensional CFD Analysis

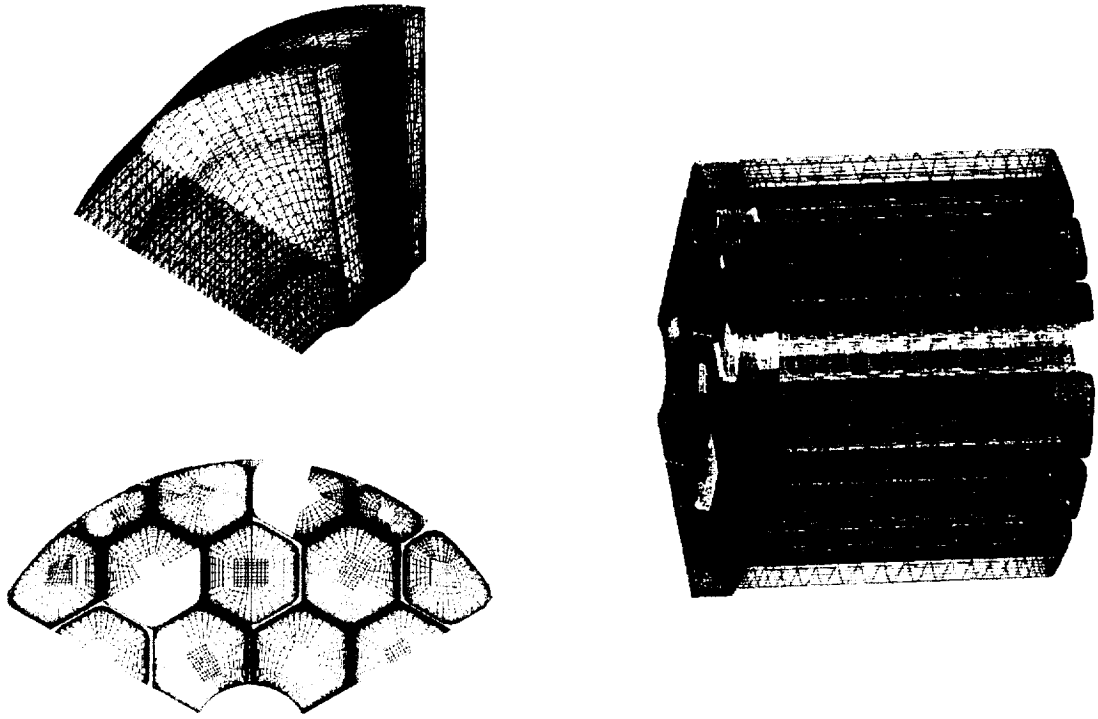

Figure 9: Three-Dimensional Computational Grid

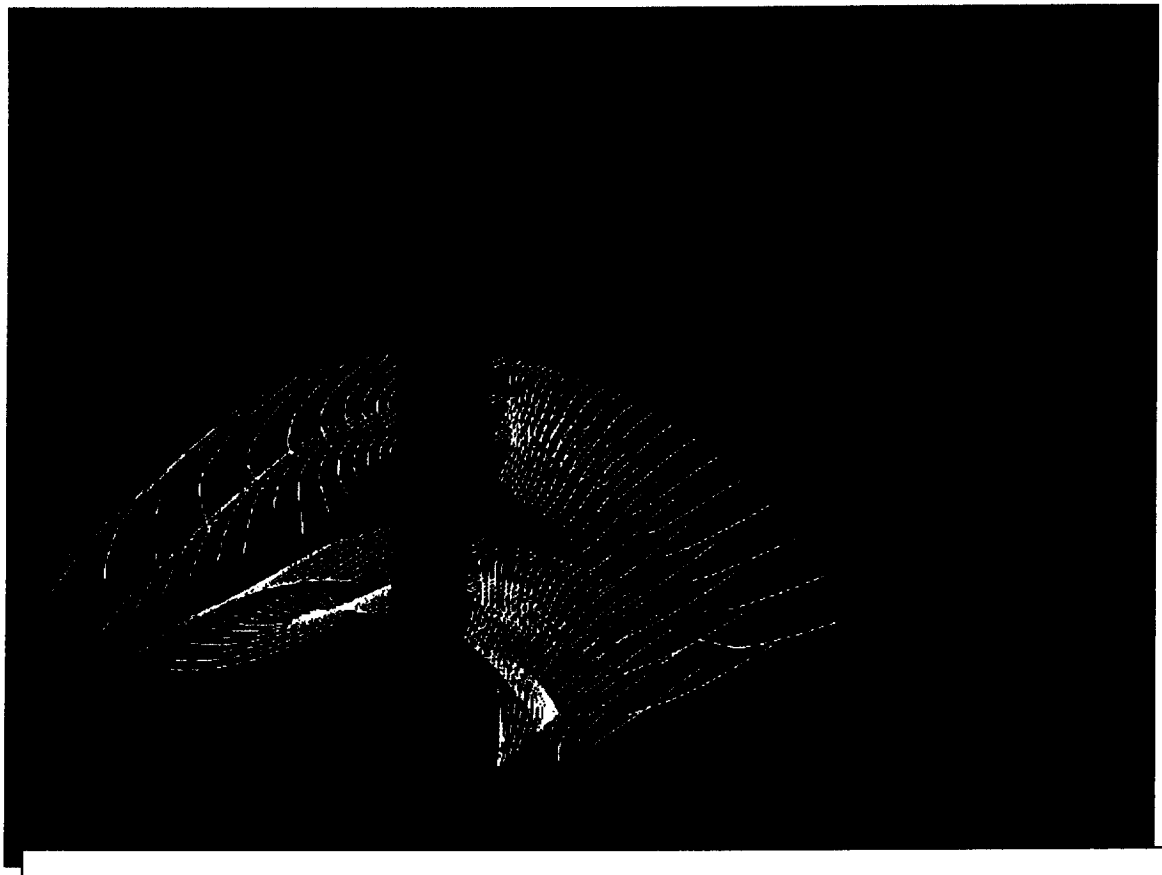

Figure 10: Flowfield Past Rotor for Existing Flowmeter

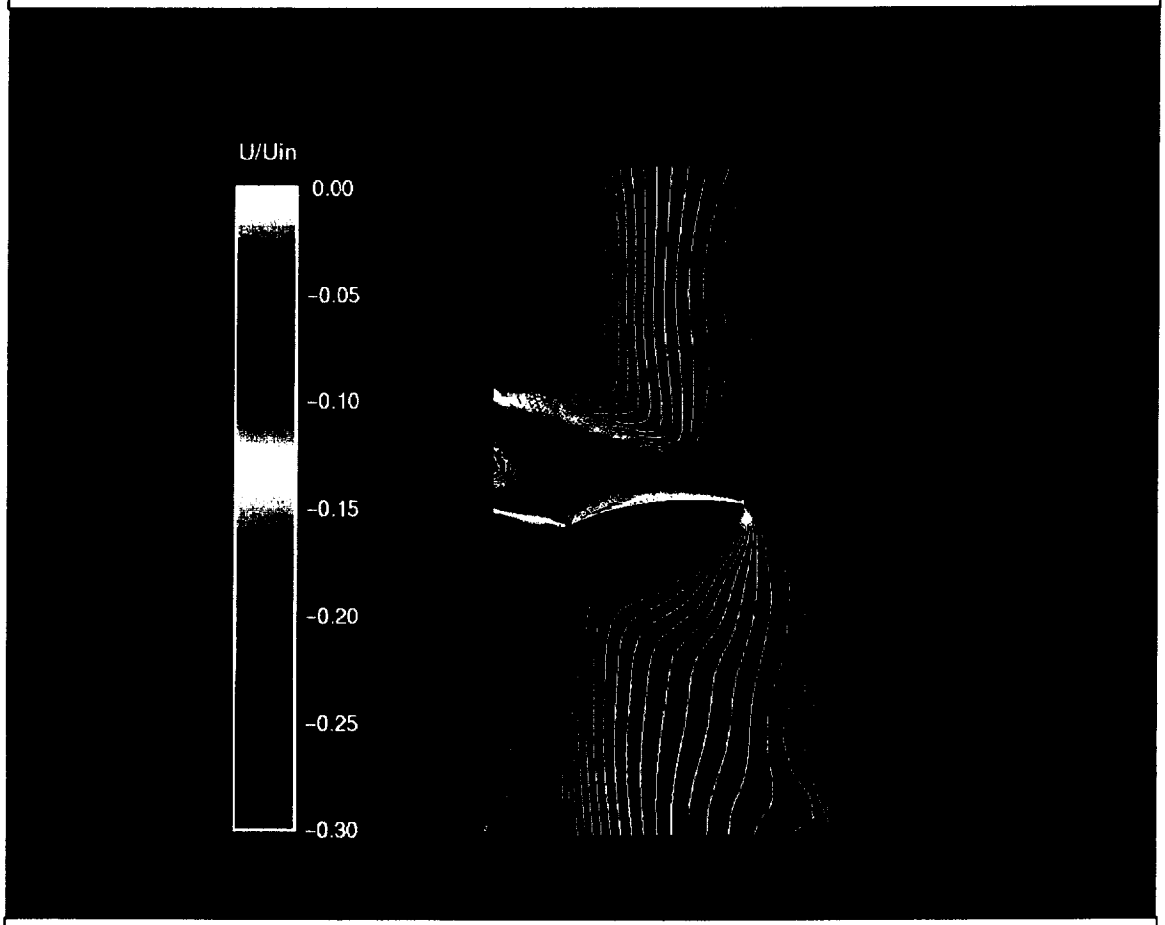

Figure 11: Velocity Field Around Rotor in Existing Flowmeter

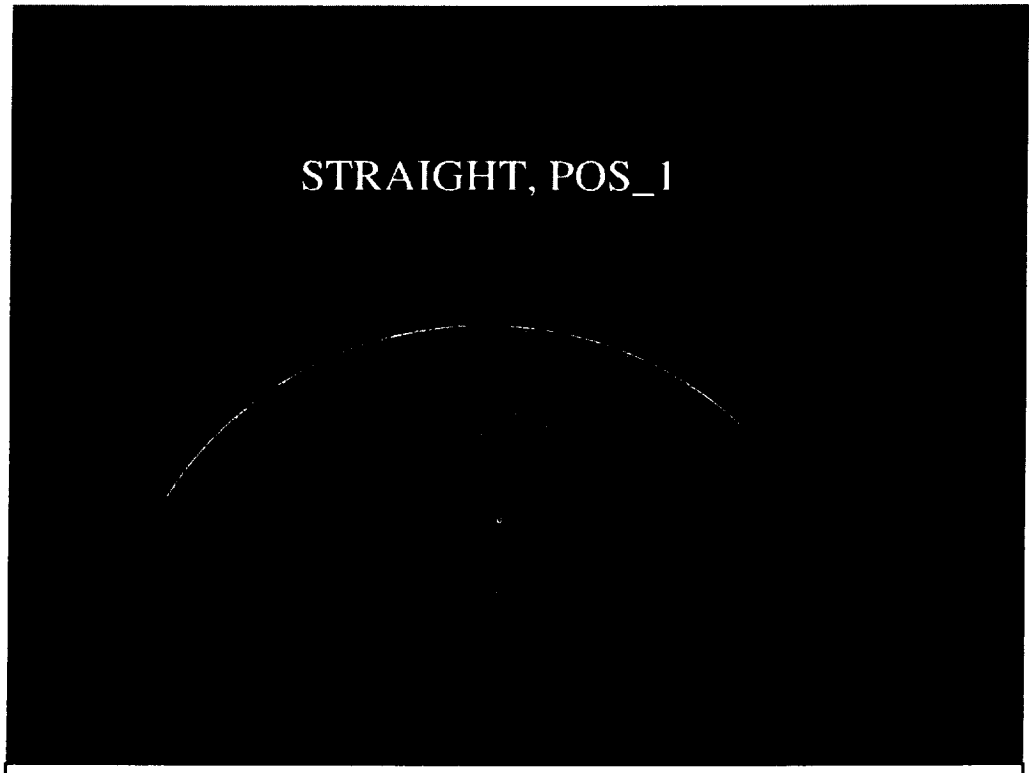

Figure 12: Wake Developed by Existing Flow Straightener

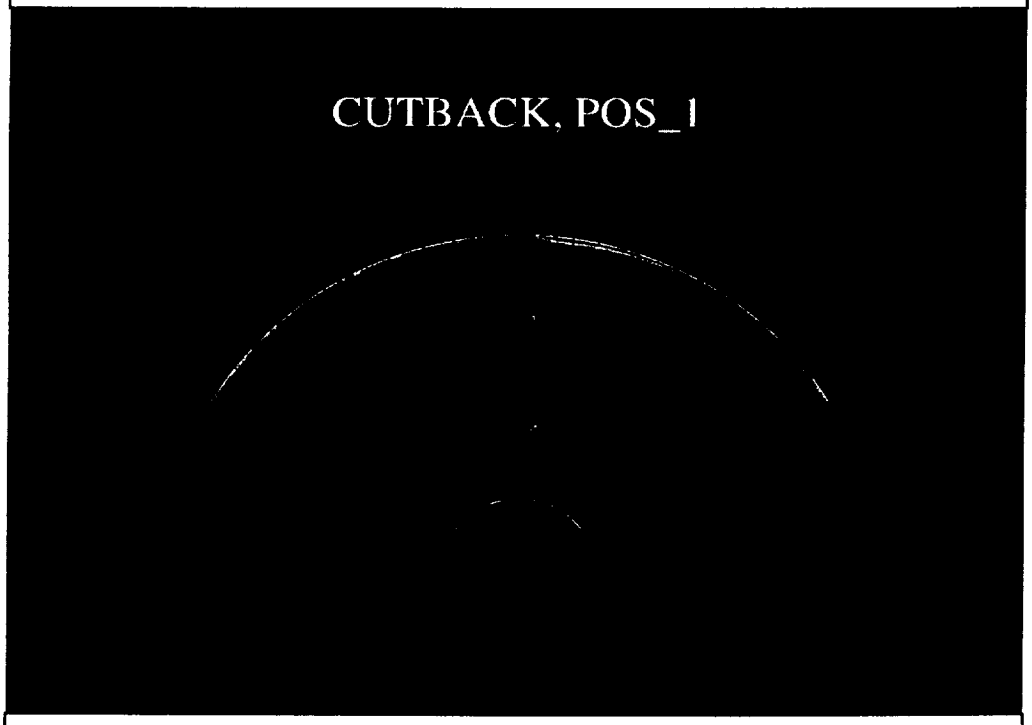

Figure 13: Wake Developed by Cutback Straightener

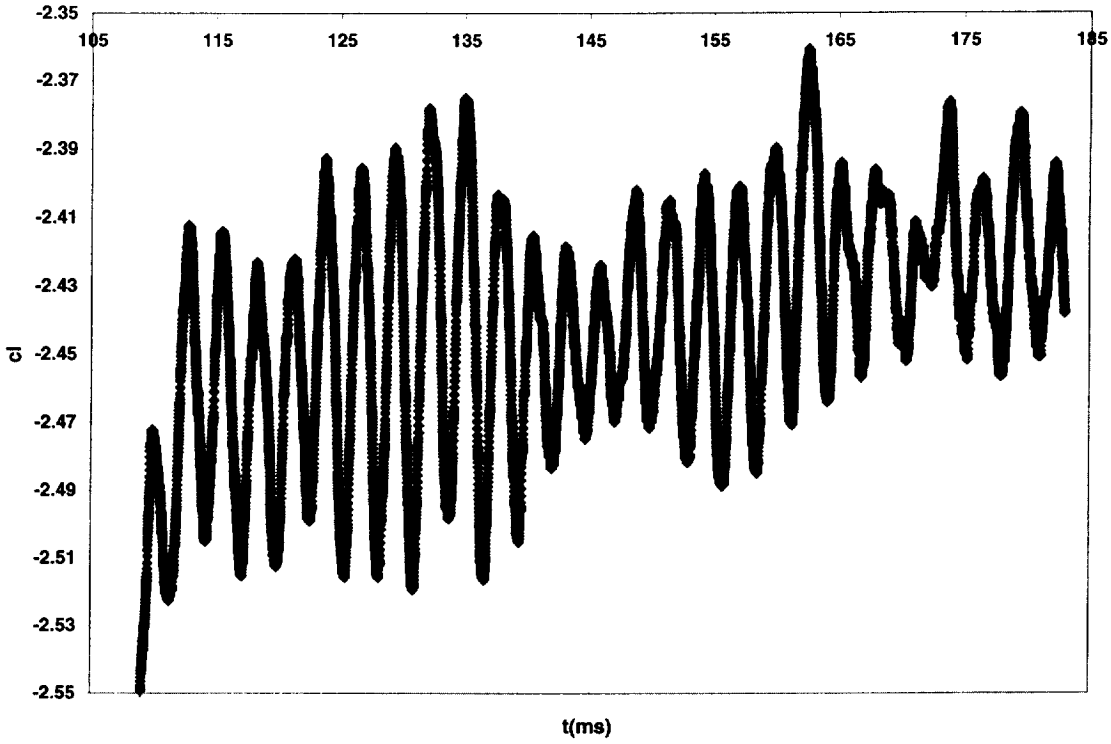

Figure 14: Lift Coefficient at Position 1 in Existing Flowmeter

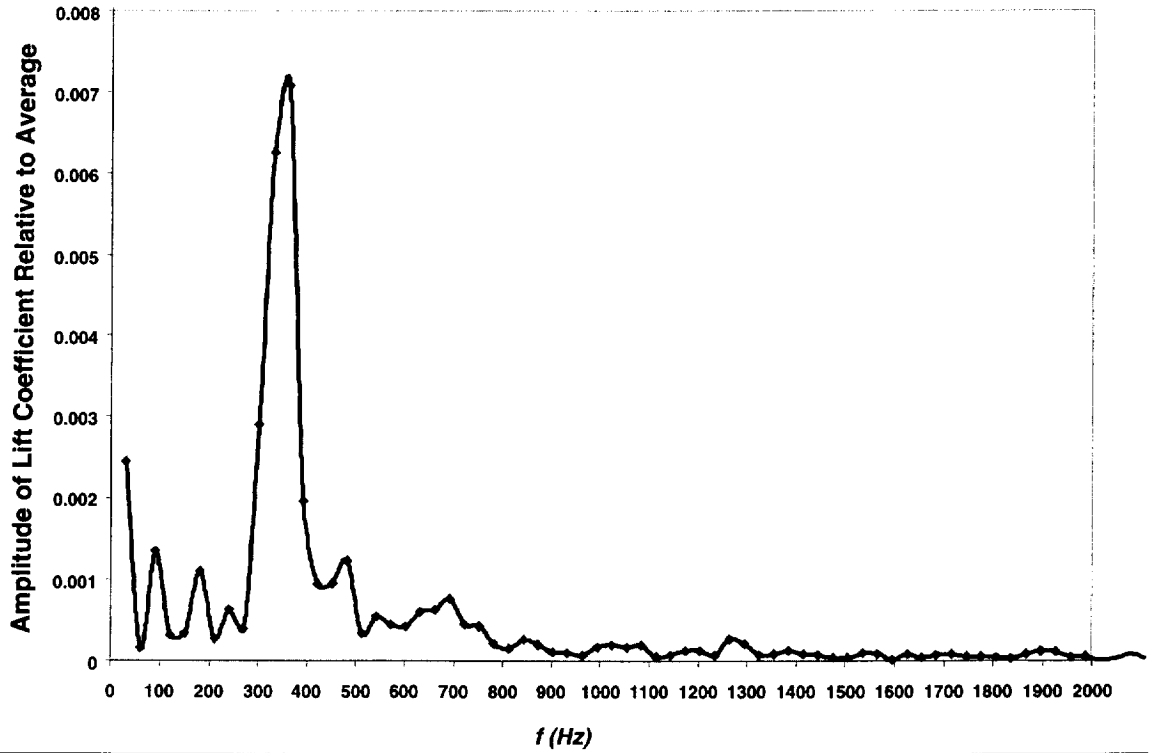

Figure 15: Power Spectral Density of Lift for Existing Flowmeter

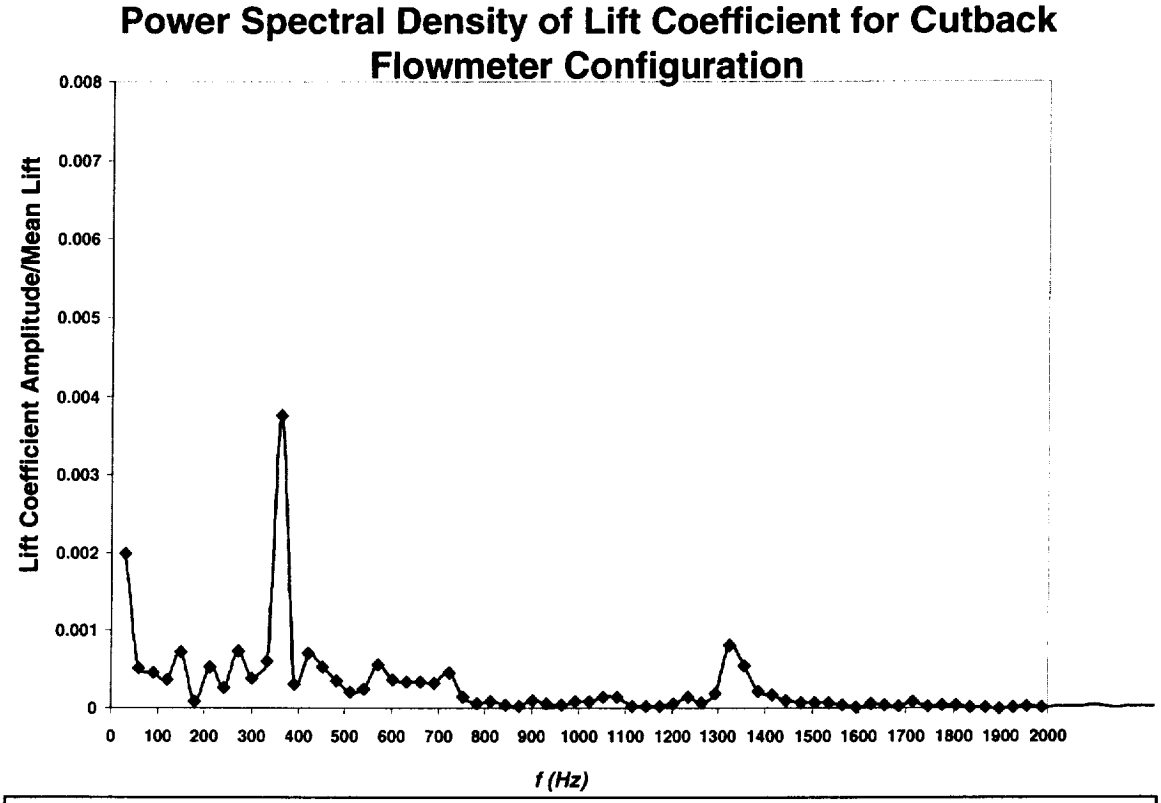

Figure 16: Power Spectral Density of Lift for Cutback Flowmeter

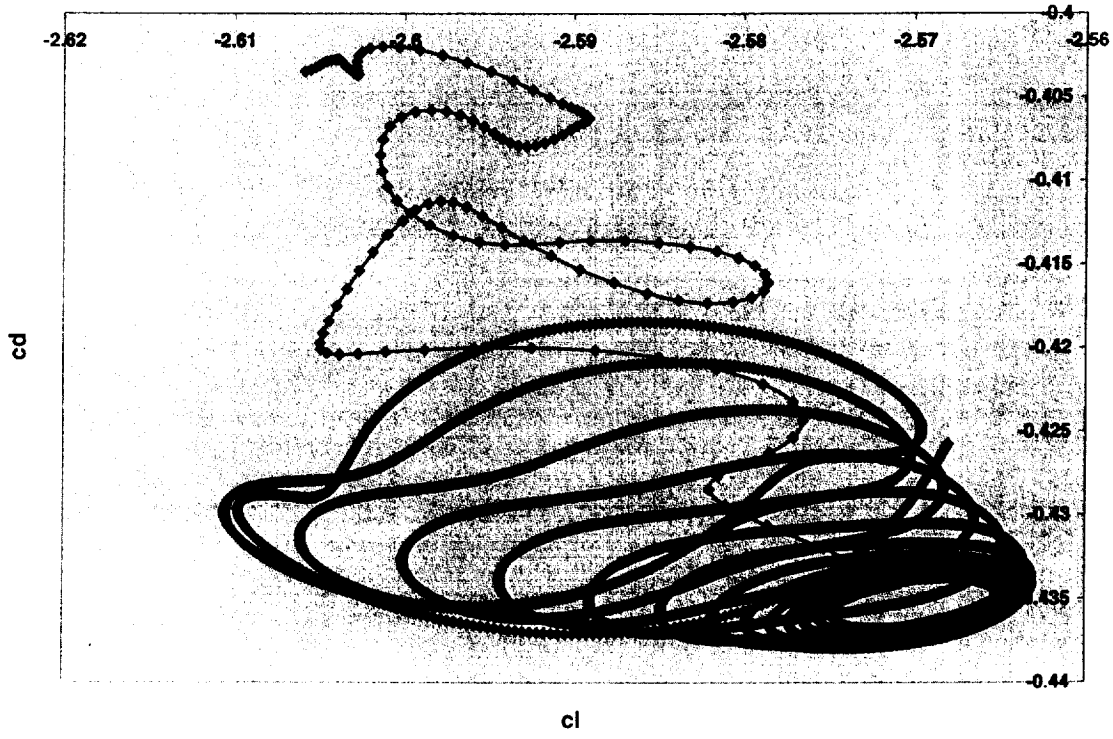

Figure 17: Drag vs. Lift for Position 2 in Existing Flowmeter